Direct Dynamics Study on the Reaction of N_2H_4 with F Atom: A Hydrogen Abstraction Reaction?

Xin Zhang and Qian Shu Li*

School of Chemistry and Environment, South China Normal University, Guangzhou 510631, People's Republic of China, and The Institute for Chemical Physics, Beijing Institute of Technology, Beijing 100081, People's Republic of China

Received: June 7, 2006; In Final Form: August 1, 2006

We present a systematic direct ab initio dynamics investigation of the reaction between N_2H_4 and F atom, which is predicted to have three possible reaction channels. The structures and frequencies at the stationary points and the points along the minimum energy paths (MEPs) of all reaction channels were calculated at the UB3LYP/6-31+G(d,p) level of theory. Energetic information of stationary points and the points along the MEPs was further refined by means of the CCSD(T)/aug-cc-pVTZ method. The calculated results revealed that the first two primary channels ($N_2H_4 + F \rightarrow N_2H_3 + HF$) are equivalent and occur synchronously via the formation of a pre-reaction complex with C_s symmetry rather than via the direct H abstraction. The pre-reaction complex then evolves into a hydrogen-bonding intermediate through a transition state with nearly no barrier and a high exothermicity, which finally makes the intermediate further decompose into N_2H_3 and HF. Another reaction channel of minor role ($N_2H_4 + F \rightarrow NH_2F + NH_2$) was also found during the calculations, which has the same C_s pre-reaction complex but forms NH_2F and NH_2 via another transition state with high-energy barrier and low exothermicity. The rate constants of these channels were calculated using the improved canonical variational transition state theory with the small-curvature tunneling correction (ICVT/SCT) method. The three-parameter ICVT/SCT rate constant expressions of $k^{ICVT/SCT}$ at the CCSD(T)/aug-cc-pVTZ//UB3LYP/6-31+G(d,p) level of theory within 220−3000 K were fitted as $(7.64 \times 10^{-9})T^{-0.87}\exp(1180/T)$ cm^3 mole^{-1} s^{-1} for $N_2H_4 + F \rightarrow N_2H_3 + HF$ and $1.45 \times 10^{-12}(T/298)^{2.17}\exp(-1710/T)$ cm^3 mole^{-1} s^{-1} for $N_2H_4 + F \rightarrow NH_2F + NH_2$.

Introduction

Hydrazine (N_2H_4), methylhydrazine (CH_3NHNH_2), and unsymmetrical dimethylhydrazine ($(CH_3)_2NNH_2$) are at present attracting growing interest as an important class of diamine-based rocket fuels.[1] These propellants are usually utilized with different oxidizers in rocket motors to generate the desired thrust. As compared to the conventional earth-storable bipropellant (N_2O_4/CH_3NHNH_2), the combination of fluorine and hydrazine (F_2/N_2H_4) has been selected as the most attractive space-storable bipropellant[2] to provide the necessary spacecraft propulsion for a wide variety of scientifically interesting unmanned planetary explorations due to its extremely large specific impulse (I_{sp}) and the very high condensed density.[3]

F_2 and N_2H_4 are both highly reactive species. N_2H_4 is one of the rare endothermic compounds, whose decomposition can lead to self-ignition,[4] detonation,[4,5] or a stable flame without any oxidizer. To accurately model the combustion of F_2/N_2H_4 bipropellants, either the decomposition mechanisms or the kinetics of the reactions involved are required. Yet most of the reaction rates in these schemes are just estimated. Only some initial decomposition reaction rates and a few rate constants of hydrazine with atom and radical reactions[6−11] have been measured. Among them, the reaction of N_2H_4 with F atom is quite important because it is one of the chain propagation steps in the flame and pyrolytic decomposition of F_2/N_2H_4 bipropellants and can provide an uncomplicated probe of chemical reactivity.

* Corresponding author. Fax: +86-10-68912665. E-mail: qsli@bit.edu.cn.

In the past several decades, almost all of the related experiments[9−11] have demonstrated that the reaction of N_2H_4 with F atom mainly proceeds via the following channel:

$$N_2H_4 + F \rightarrow N_2H_3 + HF$$

However, an anomalous experimental phenomenon[9−11] that the nascent vibrational energy disposal to HF product of $N_2H_4 + F$ reaction determined by the infrared chemiluminescence method is considerably lower than those of the other nitrogen hydrides' reactions[11] with atomic fluorine suggests this reaction proceeds by another unclear mechanism. Wategaonkar and Setser[11] suggested that the result was related to the considerable radical stabilization energy during the hydrogen abstraction. Douglas and Sloan[10] speculated that it was probably due to the influence of attractive interaction between F atom and a specific site on the N_2H_4 molecule, which could lead to a F-addition-HF-elimination pathway. Duewer[9] also proposed another possible channel for this reaction involving N−N bond fission in hydrazine:

$$N_2H_4 + F \rightarrow NH_2F + NH_2$$

and pointed out that this channel might play a certain role in this strange phenomenon. Until now, no definitive conclusions about the surprising reaction of N_2H_4 with F atom have been drawn. Also, to the best of our knowledge, little theoretical attention has been paid to this important reaction.

In the present work, we report a direct ab initio dynamics[12] study on the reaction of N_2H_4 with F atom, and the detailed

10.1021/jp063540c CCC: $33.50
Published on Web 09/23/2006

discussions and analyses are also given for the purpose of providing a clear and elaborate mechanism description of this puzzling reaction theoretically.

Methodology

A. Electronic Structure Calculations. By means of the Gaussian 03 program,[13] DFT and ab initio calculations were carried out for stationary points (reactants, complexes, transition states, and products) in an effort to obtain electronic structure information for the title reaction. The geometries of the stationary points were fully optimized employing the hybrid functional UB3LYP[14] and UMP2[15] methods with the 6-31+G(d,p) basis set, respectively. Here, B3LYP refers to the combination of Becke's three-parameter exchange with Lee−Yang−Parr (LYP) correlation functional, and UMP2 stands for the unrestricted second-order Møller−Plesset perturbation theory with frozen core approximation. The harmonic vibrational frequencies were calculated at the same two levels to identify the obtained stationary points as either equilibrium structures or transition states. Meanwhile, UQCISD/6-311+G(d,p)[16] was also used to calculate the stationary point properties of the reaction with the aim to examine the influence of electronic correlation on the geometrical parameters. To yield a more reliable potential energy surface, the single-point energies of all stationary points were further refined by means of the CCSD(T)/aug-cc-pVTZ[17] method based on the geometries at the UB3LYP/6-31+G(d,p) level. Here, CCSD(T) denotes the coupled cluster calculations including single and double substitutions with the noniterative triple excitation contributions to the energy added. In addition, the single-point energies of stationary points at the G3//UMP2/6-31+G(d,p)[18] and HL//UQCISD/6-311+G(d,p)[19] levels of theory were also calculated for comparison, which are both high accuracy single-point multilevel energy calculations with the predefined hybrid of QCISD(T), MP*n*, and HF for the G3 theory and the combination of QCISD(T) and MP2 in the HL method.

B. Reaction Path Calculations. The title reaction is substantially exothermic, which suggests a low and/or broad potential energy barrier. One consequence of a low, broad potential energy barrier for a reaction is that the rate may be controlled by different parts of the potential energy surface at different temperatures. Therefore, instead of locating only the saddle point on the potential energy surface, it is often necessary to obtain potential energy surface information in a wide vicinity of the energy barrier to determine the true dynamic bottleneck and obtain the accurate reaction rates. For this reason, the minimum energy paths (MEPs) of the reaction were obtained at the UB3LYP/6-31+G(d,p) level of theory using the intrinsic reaction coordinate (IRC) method[20] with a step size of 0.02 $(amu)^{1/2}$ bohr in mass-weighted internal coordinates. Also, several points along the MEPs were selected to compute the matrix of force constants and to perform the generalized normal-mode analysis at the same level. The single-point energies of these selected points along the MEPs were further refined at the CCSD(T)/aug-cc-pVTZ level of theory, and the ground-state vibrationally adiabatic potential energy curve was calculated by adding the vibrational zero-point energy (ZPE) to the CCSD(T) energy at each selected point along the MEPs. In this way, the $3N - 7$ harmonic vibrational frequencies, Hessian matrixes, and the high-level energies at the selected points along the MEPs were obtained to use as input to the rate constant calculations.

C. Rate Constant Calculations. The rate constant calculations were carried out employing the POLYRATE 8.2[21] program. For the purpose of comparison, the reaction rate constants were obtained using the conventional transition-state theory (TST) and the improved canonical variational transition-state theory (ICVT).[22] As a modification of the canonical variational transition-state theory (CVT),[23,24] the ICVT is implemented with the features from the microcanonical ensemble and becomes more accurate for the calculations of rate constants in low temperatures where the contribution from the threshold region is important. Within the framework of ICVT, the improved generalized transition-state rate constant, $k^{IGT}(T,s)$, can be calculated at the reaction coordinate s along the MEP at a fixed temperature; then the ICVT rate constant is obtained by minimizing $k^{IGT}(T,s)$ along the MEP at the given temperature as follows:

$$k^{ICVT}(T) = \min_s k^{IGT}(T,s)$$

in which

$$k^{IGT}(T,s) = [h\phi^R(T)]^{-1} \int_{V_a^G}^{\infty} e^{-\beta E} N^{GT}(E,s)\, dE$$

where h is Planck's constant, $\phi^R(T)$ is the reactant partition function per unit volume, $\beta = 1/(k_B T)$, k_B is Boltzmann's constant, V_a^G is the ground-state vibrationally adiabatic potential energy at s, and $N^{GT}(E,s)$ is the quantized cumulative reaction probability at energy E and reaction coordinate s.

Furthermore, in the present study, the ICVT rate constants were also corrected with the small-curvature tunneling (SCT) correction method proposed by Truhlar and co-workers,[24,44] which is based on the centrifugal dominant small-curvature semiclassical ground-state (CD-SCSAG) method and takes the quantum effects along the reaction coordinate into consideration.

Results and Discussion

The optimized geometric parameters of all reactants, complexes, products, and transition states involved in the title reaction at the UB3LYP/6-31+G(d,p), UMP2/6-31+G(d,p), and UQCISD/6-311+G(d,p) levels of theory as well as the available experimental data[25−28] are shown in Figure 1. The harmonic vibrational frequencies and ZPEs (not scaled) for all stationary points calculated at the same levels of theory are listed in Table 1. Figure 2 presents the schematic diagram of all of the predicted possible reaction channels along with the relative energies (as compared to the separate N_2H_4 and F atom) of all stationary points at the CCSD(T)/aug-cc-pVTZ//UB3LYP/6-31+G(d,p) level of theory, where reaction coordinate is schematically shown.

In the present work, the direct H abstraction of N_2H_4 by F atom was tried by various means. However, these attempts failed in the end at all of the above three levels of theory. When the distance between F and H atoms decreases, the F atom gradually turns toward the N atom of N_2H_4, forming the pre-reaction complex CMR, from which it can be suggested that there does not exist the direct hydrogen abstraction channel for the title reaction at the three levels of theory mentioned above. As shown in Figure 2, three possible reaction channels were found during the calculation. Also, from Figure 1, it is worth noting that the transition states TS1(a) and TS1(b) are actually mirror images of each other, which leads to the equivalence of channel 1 and channel 2 as well as the mirror image of the complexes CMP(a) and CMP(b) connected via a C_s transition state TS3 or TS4 through the rotation of HF group around the N−N bond in the N_2H_3 moiety. Thereby, for the sake of simplicity and clarity, the detailed calculating information is mainly provided for

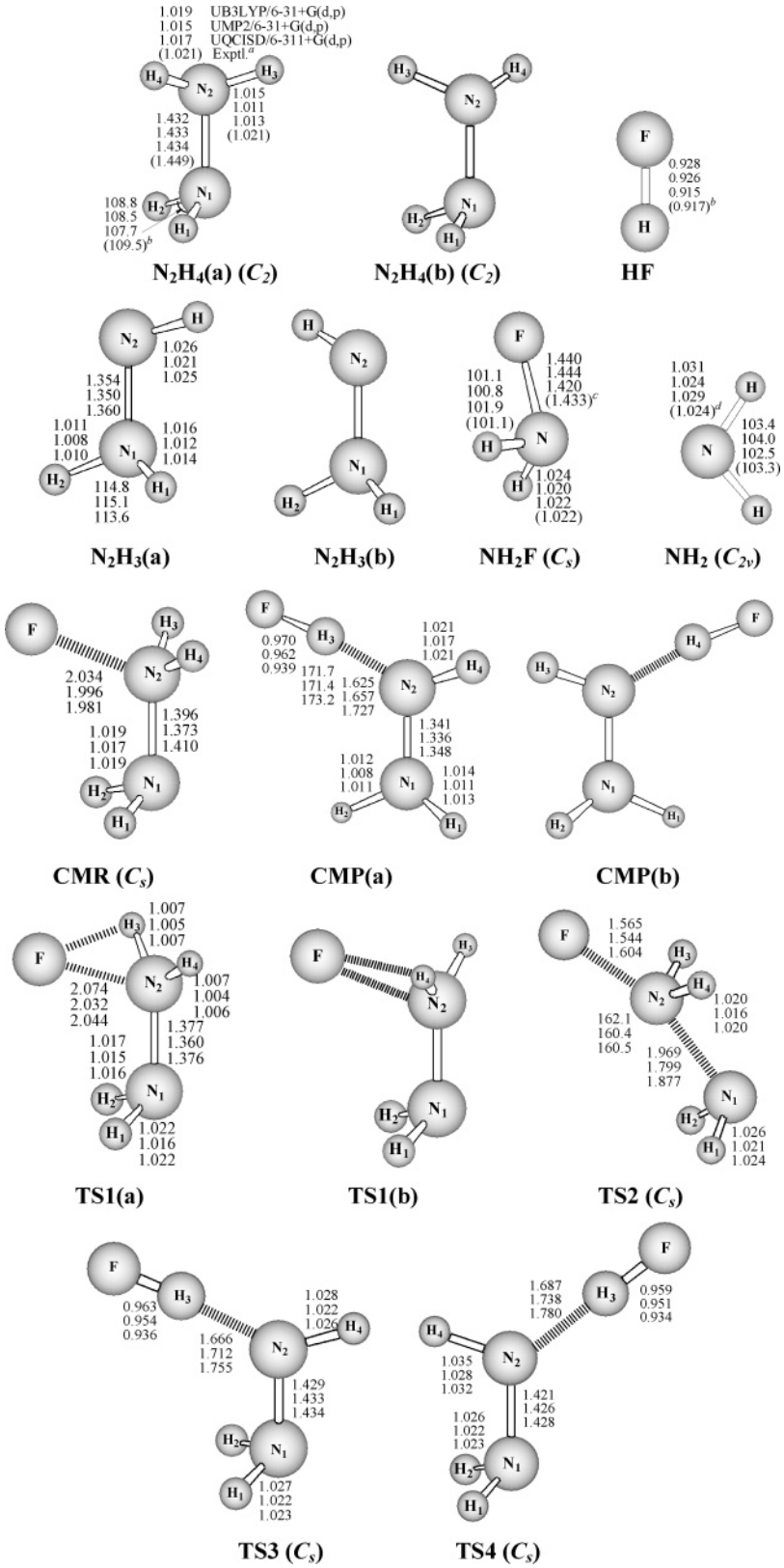

Figure 1. Conformations of reactants (stable stereoisomers of N_2H_4), complexes (CMR and stable stereoisomers of CMP), and products (HF, NH_2F, NH_2, and stable stereoisomers of N_2H_3) and structures of possible transition states for the title reaction. (Distances are in angstroms and angles are in deg.) (*a*) Reference 25. (*b*) Reference 26. (*c*) Reference 27. (*d*) Reference 28.

channels 1 and 3, and the corresponding mechanisms of the title reaction are described as follows.

I. From the Reactants to CMR. The process represented by the portion of the energy profile from the reactants to the pre-reaction complex CMR (see Figure 2) forms the initial reaction step of the title reaction. This step is exothermic and has no transition state. As the F atom and N_2H_4 approach each other, the spontaneous formation of the pre-reaction complex CMR ($^2A_1$) may be attributed to the electron donation from the lone pair of the N atom in N_2H_4 to the half-empty p orbital of F atom. From Figure 1, it can be seen that the optimized geometries of CMR at the UB3LYP/6-31+G(d,p), UMP2/6-31+G(d,p),

TABLE 1: Harmonic Vibrational Frequencies (cm^{-1}) of the Equilibriums and Transition States at the UB3LYP/6-31+G(d,p), UMP2/6-31+G(d,p), and UQCISD/6-311+G(d,p) Levels and Zero-Point Energies (kcal/mol) at the UB3LYP/6-31+G(d,p) Level (Not Scaled)

	harmonic vibrational frequencies				
	UB3LYP/6-31+G(d,p)	UMP2/6-31+G(d,p)	UQCISD/6-311+G(d,p)	exptl	ZPE
N_2H_4(a)	464, 798, 955, 1117, 1292, 1321, 1681, 1699, 3466, 3473, 3584, 3588	458, 859, 1013, 1148, 1320, 1352, 1712, 1732, 3560, 3563, 3689, 3691	440, 891, 1037, 1143, 1329, 1358, 1688, 1713, 3501, 3512, 3610, 3614	371, 896, 914, 1035, 1284, 1285, 1579, 1598, 3274, 3293, 3334, 3336[a]	33.5
N_2H_4(b)	same as N_2H_4(a)				
CMR	99, 132, 305, 417, 635, 985, 1077, 1194, 1468, 1637, 1705, 3477, 3566, 3572, 3706	107, 132, 297, 476, 925, 1072, 1185, 1489, 1639, 1735, 1855, 3553, 3656, 3757, 3840	134, 136, 344, 448, 827, 1033, 1098, 1217, 1501, 1638, 1710, 3501, 3571, 3581, 3688		34.3
CMP(a)	75, 145, 298, 504, 670, 882, 1013, 1167, 1311, 1469, 1670, 3184, 3501, 3518, 3664	70, 153, 273, 547, 722, 884, 1008, 1184, 1373, 1502, 1710, 3325, 3601, 3610, 3766	69, 152, 251, 645, 717, 822, 935, 1181, 1293, 1502, 1689, 3510, 3552, 3660, 3685		33.0
CMP(b)	same as CMP(a)				
HF	4068	4119	4212	4139[b]	5.8
N_2H_3(a)	540, 700, 1136, 1238, 1476, 1670, 3419, 3490, 3651	573, 747, 1160, 1291, 1504, 1710, 3538, 3596, 3761	638, 727, 1159, 1238, 1501, 1685, 3446, 3538, 3678		24.8
N_2H_3(b)	same as N_2H_3(a)				
NH_2F	927, 1252, 1329, 1618, 3411, 3519	950, 1287, 1341, 1648, 3505, 3630	959, 1290, 1361, 1630, 3450, 3548		17.2
NH_2	1519, 3352, 3454	1553, 3481, 3603	1558, 3420, 3529	1497, 3220, 3325[b]	11.9
TS1(a)	64, 137, 214, 420, 961, 1058, 1214, 1438, 1629, 1697, 3460, 3583, 3630, 3783, 489i	55, 98, 152, 499, 948, 1082, 1255, 1476, 1659, 1731, 3561, 3678, 3702, 3863, 644i	64, 111, 179, 456, 995, 1071, 1238, 1465, 1643, 1708, 3481, 3600, 3643, 3784, 508i		33.3
TS1(b)	same as TS1(a)				
TS2	263, 270, 394, 520, 724, 814, 1226, 1287, 1516, 1568, 3417, 3489, 3518, 3604, 702i	331, 341, 467, 712, 903, 934, 1354, 1407, 1544, 1620, 3519, 3568, 3640, 3702, 1032i	280, 282, 404, 495, 835, 910, 1230, 1303, 1510, 1574, 3444, 3505, 3537, 3612, 803i		32.3
TS3	81, 162, 274, 875, 938, 1019, 1073, 1179, 1376, 1628, 3311, 3388, 3412, 3451, 1113i	77, 184, 248, 865, 914, 1052, 1104, 1218, 1403, 1663, 3479, 3491, 3537, 3576, 802i	72, 172, 241, 814, 872, 1042, 1104, 1204, 1397, 1638, 3435, 3449, 3506, 3730, 962i		31.7
TS4	102, 143, 246, 853, 892, 983, 1062, 1167, 1365, 1605, 3283, 3374, 3390, 3463, 1209i	96, 166, 222, 842, 870, 1030, 1095, 1204, 1400, 1644, 3427, 3471, 3559, 3584, 857i	92, 150, 218, 784, 840, 1032, 1086, 1193, 1398, 1618, 3342, 3423, 3508, 3786, 994i		31.3

[a] Reference 35. [b] Reference 26.

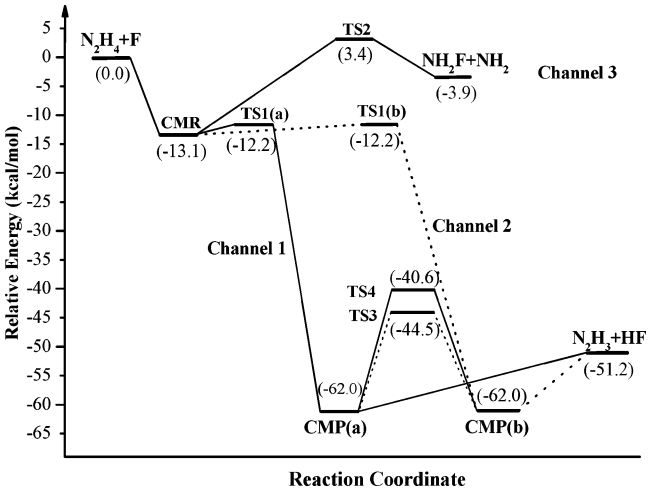

Figure 2. Schematic CCSD(T)/aug-cc-pVTZ//UB3LYP/6-31+G(d,p) potential energy profile for the reaction of N_2H_4 with F atom along with the relative energies (kcal/mol) of all stationary points in parentheses (including the ZPE and thermal corrections to 298.15 K).

and UQCISD/6-311+G(d,p) levels of theory are all very similar, each of which exhibits the C_s symmetry with the F atom and two N atoms lying in the symmetry plane. The F−N bond length in CMR is predicted to be 2.034 Å at the UB3LYP/6-31+G(d,p) level, which is much shorter than the sum (2.85 Å) of the van der Waals radii of F and N atoms but a little longer than the normal F−N covalent bond length (1.51 Å). In addition, the $\langle S^2 \rangle$ values at the above three levels of theory are all less than 0.76, indicating a rather low spin contamination.

It has been shown experimentally[25,29] and theoretically[30] that there are only two stable stereoisomers for the N_2H_4 molecule (Figure 1), which are mirror images of each other and both gauche conformations with C_2 symmetry. Yet when F atom attacks either stereoisomer, the N_2H_4 molecule will gradually turn to the reverse conformation to be convenient for associating with F atom to form the CMR with the unique C_s conformation. Therefore, this initial step makes the stereoisomer effect of N_2H_4 disappear, which is an important effect in many other N_2H_4 reactions.[31]

II. Channel 1 (or 2) from CMR to N_2H_3 + HF. This reaction channel from the pre-reaction complex CMR to products N_2H_3 + HF consists of two reaction steps: (i) the formation of the F−H bond in CMR, leading to the complex FH−N_2H_3 (CMP(a)) via a transition state TS1(a), and (ii) the rupture of the H−N bond in CMP(a), leading to products N_2H_3 + HF with no barrier. The relative simplicity of the second step makes us pay more attention to step (i).

TABLE 2: Reaction Enthalpies (ΔH_{298}^0), Global (ΔV), and Local ($\Delta V^{\ddagger}$) Potential Barriers[a] (kcal/mol) for the Possible Reaction Channels

	channel 1 or 2			channel 3		
	ΔH_{298}^0	ΔV	$\Delta V^{\ddagger}$	ΔH_{298}^0	ΔV	$\Delta V^{\ddagger}$
UB3LYP/6-31+G(d,p)	−54.51	−31.39	−0.26	−5.80	−4.93	26.19
UMP2/6-31+G(d,p)	−52.57	−21.46	−1.07	−2.87	11.40	31.80
UQCISD/6-311+G(d,p)	−49.69	−13.74	0.95	0.04	11.40	26.09
G3//UMP2[b]	−54.14	−19.29	0.31	−5.07	3.69	24.12
HL//UQCISD[c]	−54.37	−13.57	0.88	−4.46	2.64	17.08
CCSD(T)//UB3LYP[d]	−51.23	−12.25	0.89	−3.89	3.44	16.58
experiment						
ΔH_{298}^0	−52.54[e]					
E_a	0.3[f]					

[a] $\Delta V = E(\mathrm{TS}) - E(\mathrm{N_2H_4} + \mathrm{F})$, $\Delta V^{\ddagger} = E(\mathrm{TS}) - \mathrm{E(CMR)}$, TS denotes the corresponding transition state, and each energy includes the ZPE and thermal corrections to 298.15 K. [b] G3//UMP2 denotes G3//UMP2/6-31+G(d,p). [c] HL//UQCISD denotes HL//UQCISD/6-311+G(d,p) + ΔZPE. [d] CCSD(T)//UB3LYP denotes CCSD(T)/aug-cc-pVTZ//UB3LYP/6-31+G(d,p) + ΔZPE. [e] Derived from the experimental standard formation enthalpies. [f] Reference 41.

A. Stationary Points. The calculated structural parameters of all species (especially for weakly bound complexes and transition states) involved in this channel shown in Figure 1 at the UB3LYP/6-31+G(d,p) level of theory are closer to the results at the higher level of UQCISD/6-311+G(d,p) than those obtained at the UMP2/6-31+G(d,p) level of theory in general. Where comparison is possible, the theoretical bond lengths and bond angles for the reactants and products at the UB3LYP/6-31+G(d,p) and UQCISD/6-311+G(d,p) levels are in good agreement with the experimental values,[25−28] indicating these two levels are suitable to depict the structures involved in this reaction channel.

For the complex CMP(a), the F−H bond length is predicted to be 0.970 Å at the UB3LYP/6-31+G(d,p) level, which is near the normal F−H covalent bond length (0.92 Å). However, the distance between H and N atoms in CMP(a) is 1.625 Å, which is rather shorter than the sum (2.70 Å) of the van der Waals radii of H and N atoms and much longer than the H−N covalent bond length (1.02 Å) in N_2H_4. In the process of CMP(a) formation, the FH portion shows the directional behavior with the linear contact between the F−H bond and the N atom being favored. The F−H−N angle is predicted to be 171.7° at the UB3LYP/6-31+G(d,p) level. These facts indicate that CMP(a) is a hydrogen-bonding intermediate. Here, it should be mentioned that the B3LYP method has been used to study weak hydrogen bonds by many authors[32,33] and been found generally superior to the MP2 method[32] in the quality of the results.

As shown in Figure 1, the optimized geometries of transition state TS1(a) with C_1 symmetry are very similar to those of prereaction complex CMR, only with a slantwise up-turning of the two H atoms near the F atom in TS1(a) for the convenience of forming the F−H bond. The remaining framework of CMR is little affected at the saddle point. Therefore, the transition state is reactant-like, and the reaction channel will proceed via an early transition state. This character is in accordance with the nature of exothermic reactions.[34]

From Table 1, it can be seen that the harmonic vibrational frequencies of the species calculated at the three different levels of theory are very similar, and all of them are close to the available experimental data[26,35] with the maximum relative error (about 11%) being at the frequency of 798 cm^{-1} for N_2H_4 at the UB3LYP/6-31+G(d,p) level of theory as compared to the experimental value of 896 cm^{-1}. The transition state TS1(a) has only one imaginary frequency, of which the absolute values at the three different levels of theory are 489, 644, and 508 cm^{-1}, respectively. The small value of the imaginary frequency implies that the tunneling effect of this reaction channel may be not important.

Considering that the title reaction is a radical reaction, the effect of spin contamination on the energetic calculations should be avoided as much as possible. Stanton has shown that all spin contamination is essentially removed from a coupled cluster wave function.[36] Chuang et al. have also shown that coupled cluster methods, even with unrestricted reference states, provide good approximations to energetic calculations for radical reactions.[37] Thus, in this work, the single-point energies of all species were further refined at the CCSD(T)/aug-cc-pVTZ level of theory based on the geometries optimized at the UB3LYP/6-31+G(d,p) level. The reaction enthalpies and potential barriers calculated at the other five different levels of theory, UB3LYP/6-31+G(d,p), UMP2/6-31+G(d,p), UQCISD/6-311+G(d,p), G3//UMP2/6-31+G(d,p), and HL//UQCISD/6-311+G(d,p), are also collected in Table 2, which reveal that this reaction has a large negative reaction enthalpy and is therefore highly exothermic. It should be noted that the potential barriers at the UB3LYP/6-31+G(d,p) and UMP2/6-31+G(d,p) levels are overestimated due to their poor electron correlation, while the latter three levels listed in Table 2 provide reasonable values. Also, as compared to the experimental ΔH_{298}^0 of −52.54 kcal/mol derived from the experimental standard formation enthalpies (N_2H_4, 22.70;[26] F, 18.90;[26] N_2H_3, 53.95;[38] HF, −64.89 kcal/mol[26]), the calculated result of −51.23 kcal/mol at the CCSD(T)/aug-cc-pVTZ//UB3LYP/6-31+G(d,p) level of theory is especially in good agreement with the experimental value.

As has been indicated earlier,[39,40] many radical addition reactions have negative potential barriers. Our calculation results also show that the transition state TS1(a) for this reaction channel is lower in energy than the separate N_2H_4 and F atom at all levels of theory employed. Thus, for the topological consistency of the potential energy surface (PES) of the title reaction, the presence of CMR on the PES is necessary. In addition, the predicted local ($\Delta V^{\ddagger}$) potential barrier of the reaction step from CMR to TS1(a) is only 0.89 kcal/mol at the CCSD(T)/aug-cc-pVTZ//UB3LYP/6-31+G(d,p) level of theory, which is very close to the experimental estimated apparent activation energy (E_a) of 0.3 kcal/mol[41] for the title reaction. Therefore, the CCSD(T)/aug-cc-pVTZ//UB3LYP/6-31+G(d,p) method can provide a good description of channel 1 and will be adopted for the following calculations.

B. Reaction Path Properties. Figure 3 shows the changes of the bond lengths and necessary dihedral angles for the portion of channel 1 from CMR to CMP(a) along the MEP as functions of the reaction coordinate s at the UB3LYP/6-31+G(d,p) level, where s is the signed distance from the saddle point along MEP. In the course of the reaction, the lengths of the breaking bonds

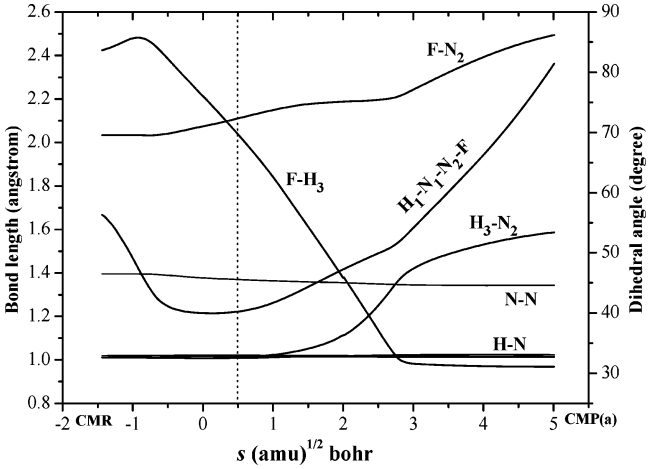

Figure 3. Changes of the bond lengths (angstroms) and dihedral angles (deg) as functions of s ((amu)$^{1/2}$ bohr) at the UB3LYP/6-31+G(d,p) level in the range from CMR to CMP(a) for channel 1.

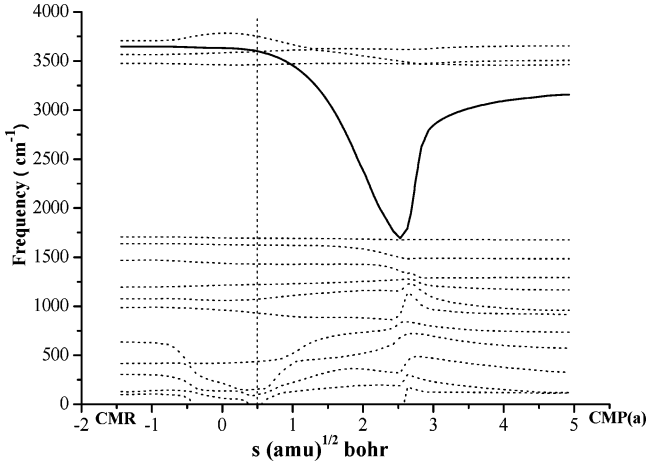

Figure 4. Changes of the generalized normal-mode vibrational frequencies (cm^{-1}) as functions of s ((amu)$^{1/2}$ bohr) at the UB3LYP/6-31+G(d,p) level in the range from CMR to CMP(a) for channel 1.

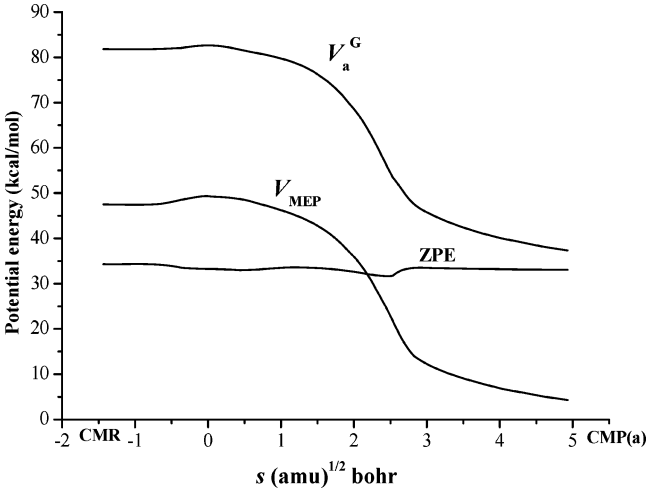

Figure 5. Classical potential energy (V_{MEP}), zero-point energy (ZPE), and ground-state vibrationally adiabatic potential energy (V_a^G) (kcal/mol) as functions of s ((amu)$^{1/2}$ bohr) at the CCSD(T)/aug-cc-pVTZ//UB3LYP/6-31+G(d,p) level in the range from CMR to CMP(a) for channel 1.

$H_{3-}N_2$ and $F-N_2$ and the forming bond $F-H_3$ as well as the dihedral angle $\Phi(H_{1-}N_{1-}N_{2-}F)$ change significantly, while the changes of other bond lengths are small. As the reaction proceeds toward CMP(a), the length of the forming bond $F-H_3$ initially has a slight increase during the slantwise up-turning of the two H atoms near the F atom in CMR from $s = -1.4$ to -0.9 (amu)$^{1/2}$ bohr and then rapidly shortens until arriving at the corresponding equilibrium F−H bond length of HF at about $s = 2.9$ (amu)$^{1/2}$ bohr. Meanwhile, the breaking bond $H_{3-}N_2$ remains insensitive up to $s = 1.0$ (amu)$^{1/2}$ bohr and then increases quickly. However, the change of the breaking bond $F-N_2$ is very peculiar, which should be understood with the analysis of the change of dihedral angle $\Phi(H_1-N_1-N_2-F)$. When the two H atoms bonded with N_2 atom in CMR turn up slantwise, F atom accordingly rotates around the N−N bond to adjust its position, which corresponds to the decrease of $\Phi(H_1-N_1-N_2-F)$ before $s = 0$ (amu)$^{1/2}$ bohr, and the length of bond $F-N_2$ is nearly invariable. As the reaction continues, the interaction between F and H_3 atoms makes the F atom rotate toward the reverse direction to approach the H_3 atom, which leads to the gradual increase of $\Phi(H_1-N_1-N_2-F)$ after $s = 0$ (amu)$^{1/2}$ bohr and the bond $F-N_2$ also begins to elongate tardily. Once the $F-H_3$ bond attains the equilibrium bond length, the dihedral angle $\Phi(H_1-N_1-N_2-F)$ increases quickly from $s = 2.9$ (amu)$^{1/2}$ bohr along with the simultaneous movement that the FH group departs from the N_2H_3 moiety until the formation of hydrogen-bonding intermediate CMP(a). It should be noted that when the reaction proceeds beyond $s = 0.5$ (amu)$^{1/2}$ bohr, all behaviors except for the change of dihedral angle $\Phi(H_1-N_1-N_2-F)$ are very similar to those of the hydrogen abstraction reactions. Also, considering the extremely low barrier height (0.89 kcal/mol) of this step, it is very easy to stride over the saddle-point TS1(a) and outstrip $s = 0.5$ (amu)$^{1/2}$ bohr. Therefore, all of these facts may enable the reaction $N_2H_4 + F \rightarrow N_2H_3 + HF$ to behave as a direct H abstraction from N_2H_4 by F atom experimentally. The attractive (hydrogen-bonding) interaction between the FH group and N_2H_3 moiety in CMP(a) is probably one of the reasons for the anomalous phenomenon of the considerably lower nascent vibrational energy disposal of HF product[9−11] in the $N_2H_4 + F$ reaction as compared to the direct H abstraction reactions of other nitrogen hydrides with F atom.

The changes of the generalized normal mode vibrational frequencies for the portion of channel 1 from CMR to CMP(a) along the MEP as functions of s at the UB3LYP/6-31+G(d,p) level are presented in Figure 4. The frequencies are associated with the pre-reaction complex CMR at $s = -1.4$ (amu)$^{1/2}$ bohr and with the hydrogen-bonding intermediate CMP(a) in the reverse limit. In the vicinity of the transition state ($s = 0$ (amu)$^{1/2}$ bohr), there are 14 vibrational frequencies, of which the frequency represented by solid line changes strongly in the range of s from 0.5 to 5.0 (amu)$^{1/2}$ bohr. When $s < 2.5$ (amu)$^{1/2}$ bohr, this vibrational mode represents the stretching vibration of the breaking bond $H-N_2$ of the molecule N_2H_4; however, when $s \geq 2.5$ (amu)$^{1/2}$ bohr, the vibrational mode relates with the stretching vibration of the forming bond F−H of the molecule HF. This kind of behavior at $s > 0.5$ (amu)$^{1/2}$ bohr again presents the similarity with hydrogen abstraction reactions.

The classical potential energy (V_{MEP}), the zero-point energy (ZPE), and the ground-state vibrationally adiabatic potential energy (V_a^G) are plotted in Figure 5 for the portion of channel 1 from CMR to CMP(a) as functions of s, which shows that the position of the maximum value of V_{MEP} at the CCSD(T)/aug-cc-pVTZ level of theory just corresponds to the saddle-point position ($s = 0$ (amu)$^{1/2}$ bohr) at the UB3LYP/6-31+G(d,p) level. Meanwhile, the maximum position of V_a^G is very close to the maximum position of V_{MEP}, and the two curves

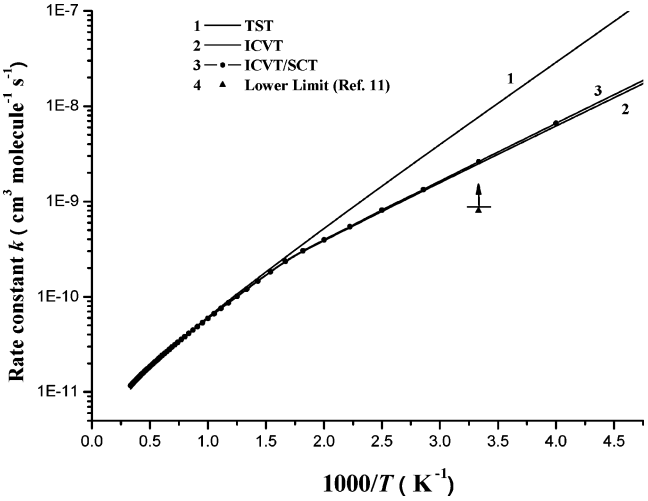

Figure 6. Plot of the TST, ICVT, and ICVT/SCT rate constants (cm^3 $mole^{-1}$ s^{-1}) at the CCSD(T)/aug-cc-pVTZ//UB3LYP/6-31+G(d,p) level versus $1000/T$ (K^{-1}) in the temperature range of 220−3000 K for channel 1.

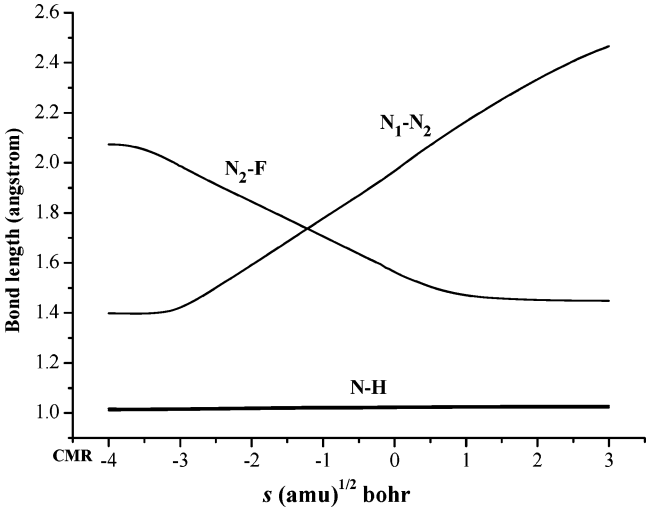

Figure 7. Changes of the bond lengths (angstroms) as functions of s ($(amu)^{1/2}$ bohr) at the UB3LYP/6-31+G(d,p) level in the range from CMR to products for channel 3.

are very similar in shape because the ZPE curve is practically constant as s varies only with a slight dip near $s = 2.5$ $(amu)^{1/2}$ bohr.

C. Rate Constant Calculation. The rate constants of channel 1 are calculated using the ICVT/SCT method at the CCSD(T)/aug-cc-pVTZ//UB3LYP/6-31+G(d,p) level of theory within a wide temperature range of 220−3000 K, which are plotted against $1000/T$ (K) in Figure 6 along with the TST and ICVT rate constants as well as available experimental data.[11] It should be noted that the rate constants of this channel obtained by all methods exhibit a negative temperature dependence. By comparing the TST rate constants with those of ICVT, it can be seen that there is a distinct difference between them at $T <$ 500 K, indicating the variational effect in rate constant calculations is important for channel 1. Meanwhile, it is not difficult to find that there only exists a slight discrepancy between ICVT and ICVT/SCT rate constants, which implies that the tunneling effect is small in the whole temperature range. In addition, our ICVT/SCT rate constant at $T = 300$ K is predicted to be 2.61×10^{-9} cm^3 $mole^{-1}$ s^{-1}, which is in good agreement with the observed lower-limit rate constant ($>4.0 \times 10^{-10}$) of the title reaction at 300 K proposed by Wategaonkar et al.[11] Finally, on the basis of the calculated ICVT/SCT rate constants within 220−3000 K at the CCSD(T)/aug-cc-pVTZ//UB3LYP/6-31+G(d,p) level of theory, a three-parameter expression $k^{ICVT/SCT} = (7.64 \times 10^{-9})T^{-0.87} \exp(1180/T)$ cm^3 $mole^{-1}$ s^{-1} is presented to describe the non-Arrhenius behavior of the rate constants for channel 1 within the broader temperature range.

III. Channel 3 from CMR to $NH_2F + NH_2$. Although there does not exist the direct H abstraction channel for the title reaction, a N abstraction channel (channel 3) has been found during our calculation (Figure 2), which has the same pre-reaction complex CMR in the entrance step discussed above. Therefore, more attention is focused on the portion of channel 3 from CMR to $NH_2F + NH_2$.

A. Stationary Points. According to the above optimized information of the stationary points for channel 1 and the calculated results of species in channel 3 shown in Figure 1, the same conclusion can be drawn that the UB3LYP/6-31+G(d,p) and UQCISD/6-311+G(d,p) methods are suitable to depict the structures involved in the reaction $N_2H_4 + F \rightarrow NH_2F + NH_2$.

As shown in Figure 1, the optimized structure of transition state TS2 has C_s symmetry like pre-reaction complex CMR. For this transition state, the three atoms involved in the bond-breaking-and-bond-forming process are nearly collinear. Comparing the geometries of TS2 with the equilibrium structures of N_2H_4 and NH_2F, it can be found that the cleaving N−N bond is stretched by 37.5% and the forming N−F bond by 8.7% at the UB3LYP/6-31+G(d,p) level. The remaining framework of NH_2F is little affected at the saddle point. Therefore, the transition state TS2 is product-like, and the channel will proceed via a late transition state, which is consistent with our expectation for a weakly exothermic reaction of channel 3 shown in Figure 2.[34]

From Table 1, it can be seen that the calculated frequencies of species in channel 3 at the UB3LYP/6-31+G(d,p) and UQCISD/6-311+G(d,p) levels are also very similar, and both are close to the corresponding experimental data.[26,35] The transition state TS2 has only one imaginary frequency, of which the absolute values at the above two levels are 702 and 803 cm^{-1}, respectively. The relatively moderate value of the imaginary frequency implies that there exists a modest tunneling effect for this reaction channel.

The calculated energetic results in Table 2 reveal that channel 3 has a low negative reaction enthalpy and is therefore weakly exothermic. The CCSD(T)/aug-cc-pVTZ//UB3LYP/6-31+G(d,p) method here is extensively adopted because of the good results of the above calculations for channel 1. No experimental value for the reaction enthalpy or energy barrier of this channel is available in the literature, but the result can be checked indirectly by comparison with the results at higher levels of theory. The reaction enthalpy ΔH_{298}^0 of channel 3 is calculated to be −3.89 kcal/mol at the CCSD(T)/aug-cc-pVTZ//UB3LYP/6-31+G(d,p) level, which is similar to the ones obtained at the G3//UMP2/6-31+G(d,p) and HL//UQCISD/6-31+G(d,p) levels. So the CCSD(T)/aug-cc-pVTZ//UB3LYP/6-31+G(d,p) method can still provide a good description for channel 3. However, it should be noted that the predicted local ($\Delta V^{\ddagger}$) barrier height of this channel at the CCSD(T)/aug-cc-pVTZ//UB3LYP/6-31+G(d,p) level is as high as 16.58 kcal/mol, which reveals that channel 3 is energetically unfeasible and might only play a minor role for the title reaction as compared to channels 1 and 2.

B. Reaction Path Properties. Figure 7 shows the changes of the bond lengths for channel 3 along the MEP as functions of s at the UB3LYP/6-31+G(d,p) level. In the course of the reaction, the lengths of the breaking bond N−N and the forming

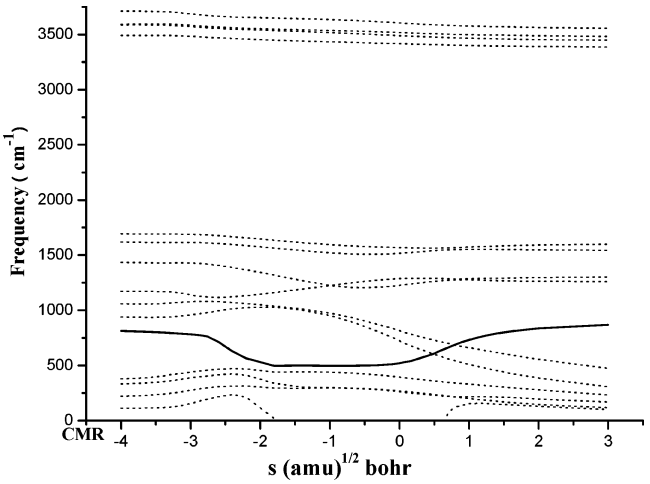

Figure 8. Changes of the generalized normal-mode vibrational frequencies (cm^{-1}) as functions of s ((amu)$^{1/2}$ bohr) at the UB3LYP/6-31+G(d,p) level in the range from CMR to products for channel 3.

bond N−F change significantly, while the changes in the other bond lengths are small. As this reaction channel proceeds to the products $NH_2F + NH_2$, the length of the breaking bond N−N remains insensitive up to $s = -3.0$ (amu)$^{1/2}$ bohr and then increases quickly. Meanwhile, the forming bond N−F rapidly shortens from CMR and arrives at the corresponding equilibrium N−F bond length of NH_2F at about $s = 1.0$ (amu)$^{1/2}$ bohr.

The changes of the generalized normal mode vibrational frequencies of channel 3 along the MEP are presented in Figure 8 as functions of s at the UB3LYP/6-31+G(d,p) level. In the vicinity of the transition state ($s = 0$ (amu)$^{1/2}$ bohr), there are 14 vibrational frequencies, of which the frequency denoted by a solid line presents the typical feature of the abstraction reactions. That is, when $s < -1.0$ (amu)$^{1/2}$ bohr, this vibrational mode represents the stretching vibration of the breaking bond N−N of the molecule N_2H_4; however, when $s \geq -1.0$ (amu)$^{1/2}$ bohr, it relates with the stretching vibration of the forming bond N−F of the molecule NH_2F. This vibrational mode can be referred to as the "reaction mode". Also, from the changes of bond lengths and frequencies, the "reaction region" of channel 3 is in the range of $s = -3.0$ to 1.0 (amu)$^{1/2}$ bohr.

Figure 9 shows the curves of V_{MEP}, ZPE, and V_a^G for channel 3. It should be noted that the position of the maximum value of the classical potential energy curve (the dotted line in Figure 9) at the CCSD(T)/aug-cc-pVTZ level does not correspond to the saddle point position ($s = 0$ (amu)$^{1/2}$ bohr) at the UB3LYP/6-31+G(d,p) level, but shifts slightly toward the reactant direction at s of approximately −0.50 (amu)$^{1/2}$ bohr. This kind of shifting is caused by the computational technique.[42,43] To ensure the accuracy of the following steps, the maximum position of $V_{MEP}(s)$ is shifted artificially to the saddle point position ($s = 0$ (amu)$^{1/2}$ bohr) (the solid line), although it can also be reoriented by the RODS algorithm[21] in the POLYRATE program. In addition, the maximum position of V_a^G is very close to the one of V_{MEP}, and the two curves are similar in shape because the ZPE curve is nearly constant as s varies.

C. Rate Constant Calculation. Figure 10 presents the calculated ICVT/SCT rate constants of channel 3 against 1000/T (K) at the CCSD(T)/aug-cc-pVTZ//UB3LYP/6-31+G(d,p) level of theory within the temperature range of 220−3000 K. For the purpose of comparison, the theories of conventional TST and ICVT are also applied to obtain the reaction rate constants in the same temperature range. It is not difficult to find that there is only a slight difference between the TST and ICVT

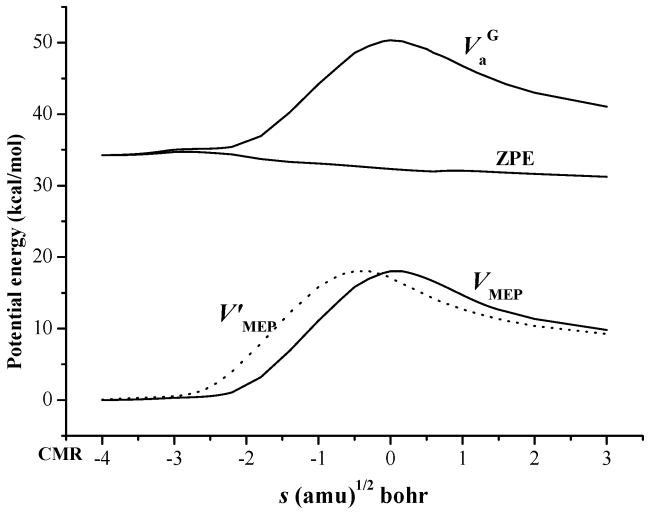

Figure 9. Classical potential energy (V_{MEP}), zero-point energy (ZPE), and ground-state vibrationally adiabatic potential energy (V_a^G) (kcal/mol) as functions of s ((amu)$^{1/2}$ bohr) at the CCSD(T)/aug-cc-pVTZ//UB3LYP/6-31+G(d,p) level in the range from CMR to products for channel 3.

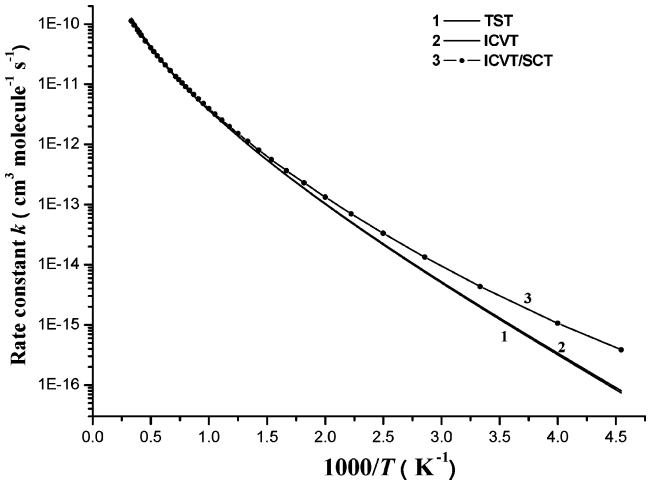

Figure 10. Plot of the TST, ICVT, and ICVT/SCT rate constants (cm^3 mole^{-1} s^{-1}) at the CCSD(T)/aug-cc-pVTZ//UB3LYP/6-31+G(d,p) level versus 1000/T (K^{-1}) in the temperature range of 220−3000 K for channel 3.

rate constants, indicating that the variational effect is small. In addition, even though the ICVT and ICVT/SCT rate constants are quite similar at $T \geq 500$ K, there are still some discrepancies between them when $T < 500$ K, which implies that there exists a moderate tunneling effect on the rate constant calculation at low temperatures. Finally, on the basis of the calculated ICVT/SCT rate constants of channel 3 within 220−3000 K at the CCSD(T)/aug-cc-pVTZ//UB3LYP/6-31+G(d,p) level of theory, a three-parameter expression $k^{ICVT/SCT} = 1.45 \times 10^{-12}(T/298)^{2.17} \exp(-1710/T)$ cm^3 mole^{-1} s^{-1} is fitted to describe the non-Arrhenius behavior of the rate constants for channel 3 within the broader temperature range.

Summary

In this work, a systematic investigation on the reaction of hydrazine with fluorine atom has been conducted by a direct ab initio dynamics method. The results show that the accurate geometry and frequency information for all species involved in the title reaction can be provided at the UB3LYP/6-31+G(d,p) level of theory and the CCSD(T)/aug-cc-pVTZ//UB3LYP/6-31+G(d,p)

method is necessary to improve the potential energy surface. According to our calculations, as the F atom and N_2H_4 approach each other, they spontaneously form the pre-reaction complex CMR with C_s symmetry in the entrance step of the title reaction rather than react directly by the H abstraction. Subsequently, the pre-reaction complex CMR evolves into a hydrogen-bonding intermediate CMP(a) via a transition state TS1(a) with nearly no barrier and an exothermicity of 48.85 kcal/mol. The high exothermicity makes CMP(a) chemically active, which further decomposes into N_2H_3 and HF with an energy of 10.76 kcal/mol consumed. The above steps form the complete mechanism of reaction $N_2H_4 + F \rightarrow N_2H_3 + HF$ with the synchronous occurring of the equivalent channels 1 and 2 (Figure 2) caused by the mirror images of transition states TS1(a) and TS1(b). Meanwhile, another reaction channel of $N_2H_4 + F \rightarrow NH_2F + NH_2$ (channel 3) has also been found during the calculations, which has the same entrance step of channel 1 but forms NH_2F and NH_2 via another transition state TS2 with a high energy barrier of 16.58 kcal/mol and a low exothermicity of 3.89 kcal/mol. The rate constants of these channels for the title reaction in the temperature range of 220−3000 K have been calculated using the ICVT/SCT method, which reveal that the variational effect is important for channels 1 and 2 and the small curvature tunneling effect is modest for channel 3 within the lower temperature range. The three-parameter ICVT/SCT rate constant expressions of all possible channels for the title reaction at the CCSD(T)/aug-cc-pVTZ//UB3LYP/6-31+G(d,p) level of theory within 220−3000 K have been fitted as $k^{ICVT/SCT} = (7.64 \times 10^{-9})T^{-0.87} \exp(1180/T)$ cm^3 mole^{-1} s^{-1} for $N_2H_4 + F \rightarrow N_2H_3 + HF$ and $k^{ICVT/SCT} = 1.45 \times 10^{-12}(T/298)^{2.17} \exp(-1710/T)$ cm^3 mole^{-1} s^{-1} for $N_2H_4 + F \rightarrow NH_2F + NH_2$, which clearly show that the more favorable reaction channels are channels 1 and 2, while channel 3 only plays a minor role in the whole temperature range. In addition, the formation of the pre-reaction complex CMR in the entrance step and the hydrogen-bonding intermediate CMP(a) in the exit step for channels 1 and 2 is probably the primary reason for the anomalous phenomenon of the considerably lower nascent vibrational energy disposal of HF product in $N_2H_4 + F$ reaction as compared to the direct H abstraction reactions of other nitrogen hydrides with F atom.

Acknowledgment. This work is supported by the National Natural Science Foundation of China. Thanks are due to Professor D. G. Truhlar for providing the POLYRATE 8.2 program. We are also grateful to our reviewers for their valuable comments on the manuscript.

References and Notes

(1) Sutton, G. P. *Rocket Propulsion Elements. An Introduction to the Engineering of Rockets*; Wiley: New York, 1992.
(2) Bond, D. L. *J. Spacecr. Rockets* **1980**, *17*, 342.
(3) Thunnissen, D. P.; Guernsey, C. S.; Baker, R. S.; Miyake, R. N. AIAA-2004-3488, 2004.
(4) Auzanneau, M.; Roux, M. *Combust. Sci. Technol.* **1990**, *73*, 505.
(5) Pedley, M. D.; Bishop, C. V.; Benz, F. J.; Bennett, C. A.; McClenagan, R. D.; Fenton, D. L.; Knystautas, R.; Lee, J. H.; Peraldi, O.; Dupre, G.; Shepherd, J. E. *AIAA Prog. Astronaut. Aeronaut.* **1988**, *114*, 45.
(6) Lindsay, D. M.; Gole, J. L.; Lombardi, J. R. *Chem. Phys.* **1979**, *37*, 333.
(7) Konnov, A. A.; Ruyck, J. D. *Combust. Flame* **2001**, *124*, 106.
(8) Vaghjiani, G. L. *Int. J. Chem. Kinet.* **1995**, *101*, 4167.
(9) Duewer, W. H.; Setser, D. W. *J. Chem. Phys.* **1973**, *58*, 2310.
(10) Douglas, D. J.; Sloan, J. J. *Chem. Phys.* **1980**, *46*, 307.
(11) Wategaonkar, S.; Setser, D. W. *J. Chem. Phys.* **1987**, *86*, 4477.
(12) Truhlar, D. G.; Gordon, M. S. *Science* **1990**, *249*, 491.
(13) Frisch, M. J.; Trucks, G. W.; Schlegel, H. B.; Scuseria, G. E.; Robb, M. A.; Cheeseman, J. R.; Montgomery, J. A., Jr.; Vreven, T.; Kudin, K. N.; Burant, J. C.; Millam, J. M.; Iyengar, S. S.; Tomasi, J.; Barone, V.; Mennucci, B.; Cossi, M.; Scalmani, G.; Rega, N.; Petersson, G. A.; Nakatsuji, H.; Hada, M.; Ehara, M.; Toyota, K.; Fukuda, R.; Hasegawa, J.; Ishida, M.; Nakajima, T.; Honda, Y.; Kitao, O.; Nakai, H.; Klene, M.; Li, X.; Knox, J. E.; Hratchian, H. P.; Cross, J. B.; Adamo, C.; Jaramillo, J.; Gomperts, R.; Stratmann, R. E.; Yazyev, O.; Austin, A. J.; Cammi, R.; Pomelli, C.; Ochterski, J. W.; Ayala, P. Y.; Morokuma, K.; Voth, G. A.; Salvador, P.; Dannenberg, J. J.; Zakrzewski, V. G.; Dapprich, S.; Daniels, A. D.; Strain, M. C.; Farkas, O.; Malick, D. K.; Rabuck, A. D.; Raghavachari, K.; Foresman, J. B.; Ortiz, J. V.; Cui, Q.; Baboul, A. G.; Clifford, S.; Cioslowski, J.; Stefanov, B. B.; Liu, G.; Liashenko, A.; Piskorz, P.; Komaromi, I.; Martin, R. L.; Fox, D. J.; Keith, T.; Al-Laham, M. A.; Peng, C. Y.; Nanayakkara, A.; Challacombe, M.; Gill, P. M. W.; Johnson, B.; Chen, W.; Wong, M. W.; Gonzalez, C.; Pople, J. A. *Gaussian 03*; Gaussian, Inc.: Pittsburgh, PA, 2003.
(14) Becke, A. D. *J. Chem. Phys.* **1993**, *98*, 1372.
(15) Frisch, M. J.; Head-Gordon, M.; Pople, J. A. *Chem. Phys. Lett.* **1990**, *166*, 275.
(16) Pople, J. A.; Head-Gordon, M.; Raghavachari, K. *J. Chem. Phys.* **1987**, *87*, 5968.
(17) Scuseria, G. E.; Schaefer, H. F., III. *J. Chem. Phys.* **1989**, *90*, 3700.
(18) Curtiss, L. A.; Raghavachari, K.; Redfern, P. C.; Rassolov, V.; Pople, J. A. *J. Chem. Phys.* **1998**, *109*, 7764.
(19) Miller, J. A.; Klippenstein, S. J. *J. Phys. Chem. A* **2003**, *107*, 2680.
(20) Gonzalez, C.; Schlegel, H. B. *J. Phys. Chem.* **1990**, *94*, 5523.
(21) Chuang, Y.-Y.; Corchado, J. C.; Fast, P. L.; Villa, J.; Hu, W.-P.; Liu, Y.-P.; Lynch, G. C.; Jackels, C. F.; Nguyen, K.; Gu, M. Z.; Rossi, I.; Coitino, E.; Clayton, S.; Melissas, V.; Lynch, B. J.; Steckler, R.; Garret, B. C.; Isaacson, A. D.; Truhlar, D. G. *POLYRATE*, version 8.2; University of Minnesota: Minneapolis, MN, 1999.
(22) Garrett, B. C.; Truhlar, D. G.; Grev, R. S.; Magnuson, A. W. *J. Phys. Chem.* **1980**, *84*, 1730.
(23) Truhlar, D. G.; Garrett, B. C. *Annu. Rev. Phys. Chem.* **1984**, *35*, 159.
(24) Truhlar, D. G.; Isaacson, A. D.; Garret, B. C. In *Theory of Chemical Reaction Dynamics*; Baer, M., Ed.; CRC Press: Boca Raton, FL, 1985; Vol. 4, p 65.
(25) Kohata, K.; Fukuyama, T.; Kuchitsu, K. *J. Phys. Chem.* **1982**, *86*, 602.
(26) Chase, M. W., Jr. *NIST-JANAF Thermochemical Tables*, 4th ed.; *J. Phys. Chem. Ref. Data* **1998**; Monograph No. 9.
(27) Christen, D.; Minkwitz, R.; Nass, R. *J. Am. Chem. Soc.* **1987**, *109*, 7020.
(28) Lide, D. R., Ed. *CRC Handbook of Chemistry and Physics*, 84th ed.; CRC Press: New York, 2003.
(29) Burenin, A. V. *Opt. Spectrosc.* **2000**, *88*, 28.
(30) (a) Ding, F. J.; Zhang, L. F. *Int. J. Quantum Chem.* **1997**, *64*, 447. (b) Dyczmons, V. *J. Phys. Chem. A* **2000**, *104*, 8263.
(31) (a) Li, Q. S.; Zhang, X.; Zhang, S. W. *J. Phys. Chem. A* **2003**, *107*, 6055. (b) Li, Q. S.; Zhang, X. *J. Chem. Phys.* **2006**, *125*, 64304.
(32) Rablen, P. R.; Lockman, J. W.; Jorgensen, W. L. *J. Phys. Chem. A* **1998**, *102*, 3782.
(33) Sun, M. *J. Chem. Phys.* **2006**, *124*, 54903.
(34) Hammond, G. S. *J. Am. Chem. Soc.* **1955**, *77*, 334.
(35) Yamaguchi, A. *Nippon Kagaku Zasshi* **1959**, *80*, 1109.
(36) Stanton, J. F. *J. Chem. Phys.* **1994**, *101*, 371.
(37) Chuang, Y.-Y.; Coitino, E. L.; Truhlar, D. G. *J. Phys. Chem. A* **2000**, *104*, 446.
(38) Armstrong, D. A.; Yu, D.; Rauk, A. *J. Phys. Chem. A* **1997**, *101*, 4761.
(39) Sekusak, S.; Liedl, K. R.; Sabljic, A. *J. Phys. Chem. A* **1998**, *102*, 1583.
(40) Brana, P.; Sordo, J. A. *J. Comput. Chem.* **2003**, *24*, 2044.
(41) Gibson, S. T.; Greene, J. P.; Berkowitz, J. *J. Chem. Phys.* **1985**, *83*, 4319.
(42) Espinosa-Garcia, J.; Corchado, J. C. *J. Phys. Chem.* **1995**, *99*, 8613.
(43) Rosenman, E.; McKee, M. L. *J. Am. Chem. Soc.* **1997**, *119*, 9033.
(44) Liu, Y.-P.; Lynch, G. C.; Truong, T. N.; Lu, D.-h.; Truhlar, D. G.; Garrett, B. C. *J. Am. Chem. Soc.* **1993**, *115*, 2408.